HHS Public Access

Author manuscript

J Mol Struct. Author manuscript; available in PMC 2020 June 29.

Published in final edited form as:

J Mol Struct. 2020 April 5; 1205: . doi:10.1016/j.molstruc.2019.127594.

A rhodamine-based fluorescent sensor for selective detection of Cu^{2+} in aqueous media: synthesis and spectroscopic properties

Fasil Abebe[*], **Pierce Perkins**, **Roosevelt Shaw**, **Solomon Tadesse**

Department of Chemistry, Morgan State University, Baltimore, MD 21251, USA

Abstract

Two new chemosensors, rhodamine B derivative bearing 3-formyl-6-nitrochromone ($\mathbf{L_1}$) and 3-formyl-6-methylchromone ($\mathbf{L_2}$) units were designed and synthesized using microwave irradiation for the selective detection of Cu^{2+} in aqueous media. Copper triggers the formation of highly fluorescent ring-open spirolactam. The fluorescence intensity was remarkably increased upon the addition of Cu^{2+} within a minute, while the other metal ions caused no significant effect. More importantly, the resulting complexes can be used as a reversible fluorescence sensor for CN^-. The recognition ability of the sensors was investigated by fluorescence titration, Job's plot, ^1H NMR spectroscopy and density functional theory (DFT) calculations.

Keywords

Microwave; Fluorescence sensor; Rhodamine; Chromone; Cu^{2+}; CN^-

1. Introduction

Copper is the third in abundance among the essential heavy metals in human bodies and plays an important role in various physiological processes. It is essential for the activation of dioxygen, which is essential for the survival of all living organisms. Copper also has multiple functions, as iron absorption, hemopoiesis, diverse enzyme activities and in the redox processes [1–2]. Abnormal levels of copper ions can lead to vomiting, lethargy, increased blood pressure, acute haemolytic anemia, neurotoxicity, and neurodegenerative disease [3–6]. Accordingly, fluorescent and colorimetric sensors for the detection of Cu^{2+} have received increasing scientific attention [7–13]. So far, various Cu^{2+} sensors have been proposed; however, most of these show a turn-off response, because Cu^{2+} usually acts as a quencher via an energy or electron–transfer process [14]. Recently, "Turn-on" types have also been reported [14–18]. However, there are some probes designed based on rhodamines, which show a fluorescence off-on response with reversible behavior upon complexation [15–16].

[*]Authors to whom correspondence should be addressed; Fasil.Abebe@morgan.edu.

Conflict of interest

The authors declared that there is no conflict of interest

Appendix A. Supplementary data

Supplementary material related to this article can be found, in the online version, at doi:

Rhodamine dyes were used to construct fluorescent sensors because of their excellent spectroscopic properties, such as long absorption and emission wavelength, high fluorescent quantum yield, large extinction coefficient, and great photostability [19–23]. Rhodamine derivatives are non-fluorescent and colorless, but ring-opening of the corresponding spirolactam produces strong fluorescence emission and a pink color [24]. This property provides an ideal model for constructing OFF-ON fluorescent sensors. The equilibrium between the two forms is highly sensitive to the pH of the medium, the ring-open form being predominant in acidic conditions. Metal ions can trigger the change in structure between the spirocyclic and ring-open form and therefore rhodamine-based compounds have been well established as sensors for metal ions [18–24].

Here, we report two new rhodamine derivatives, **L_1** and **L_2**, with different substituent groups on chromone ring designed for rapid, selective, and colorimetric sensors for Cu^{2+}, in which the spirolactam to ring-opened amide process was utilized for the detection of Cu^{2+} in aqueous media. Several studies have shown that the structure of the substituent group on the lactam ring has influence on the properties of rhodamine derivatives [25–26]. The presence of nitro ($-NO_2$) units can significantly increase the sensitivity and selectivity of chemical sensors for Cu^{2+} compared to methyl ($-CH_3$) groups. After comparison of optical properties, probe **L_1** showed a good performance in Cu^{2+} recognition, which indicated that the different electronic distributions among the sensor's structures have an influence on their properties. For this reason, we selected **L_1** as a typical example to expound in the following discussion. In this work, we present an efficient, clean, and straightforward procedure to prepare rhodamine derivatives by microwave- assisted organic synthesis under minimum solvent conditions, using ethanol as a green solvent and short reaction times.

2. Experimental

2.1. Materials and instruments

All the reagents and solvents were purchased as analytical-grade and used without further purification unless otherwise stated. Microwave-assisted organic synthesis reactions were carried out in a CEM microwave reactor. ^{1}H-NMR and ^{13}C-NMR spectra were recorded using an Avance 400 MHz NMR spectrometer (Bruker Biospin, Billerica, MA, USA). The IR spectrum was obtained using Shimadzu IRAffinity-1S FTIR spectrometer (Shimadzu Scientific, Columbia, MD, USA). All UV/Vis spectroscopy experiments were recorded using Agilent Cary 60 UV-Vis spectrometer (Agilent, Walnut Creek, CA, USA). Fluorescence emission experiments were measured using Varian Cary Eclipse fluorescence spectrophotometer (Varian, Walnut Creek, CA, USA), with excitation and emission slit widths of 5 nm and excitation wavelength at 510 nm.

2.2. Spectroscopic studies

The stock solutions of metal ions were prepared from their nitrate and chloride salts and anion species from their tetrabutylammonium salts. Distilled deionized water was used throughout the experiments. All the spectroscopic studies were performed in aqueous acetonitrile solution in which the sensors formed a colorless solution that was stable for more than a week. Stock solutions of ligands **L_1** and **L_2** (1×10^{-3} M), selected salts of cations

(1×10^{-3} M) and anions (1×10^{-4} M) were prepared in CH_3CN/H_2O. $\mathbf{L_1}$-Cu^{2+} and $\mathbf{L_2}$-Cu^{2+} solution for CN^- detection were prepared by addition of 1.0 equivalent of Cu^{2+} to the solution of both $\mathbf{L_1}$ and $\mathbf{L_2}$ (20 μM) in Tris-HCl (10 mM, pH =7.2) buffer containing CH_3CN/H_2O (7:3 v/v) solution. The resulting solution was shaken well before recording the spectra.

2.3. Fluorescence titration experiments

The fluorescence titration experiments of rhodamine derivatives (20 μM) were carried out in acetonitrile solution. Each fluorescence titration was repeated at least three times until consistent values were obtained. Jobs continuous variation method was used for determining the binding stoichiometry of the complexation reaction. The association constant (K) was calculated from absorbance studies by linear Benesi-Hildebrand equation [27]. The detection limits (DLs) of sensor for Cu^{2+} were calculated using the equation (DL=3σ/S), where σ is the standard deviation of the blank measurements and S is the slope between the emission intensity vs the concentration of copper ion.

2.4. DFT studies

Time-density functional theory (TD-DFT) calculations were employed to elucidate the Cu^{2+} interactions with $\mathbf{L_1}$ and $\mathbf{L_2}$ systems. All computations were carried out using Spartan'18 software package. Geometry optimization of the ground state structures was carried out with TD-DFT at the B3LYP level of theory using 6–31G (d, p) basis set in the gas phase and in a simulated water medium.

2.5. Microwave-assisted synthesis of L_1 and L_2

Synthesis of compound L_1: A mixture of **1** (100 mg, 0.219 mmol), 3-formyl-6-nitrochromone (48mg, 0.219 mmol), and ethanol (2 mL) was placed in a 10 mL reaction vial. The resulting mixture was stirred to make it homogeneous and it was placed in the cavity of a CEM microwave reactor. The closed reaction vessel was run under pressure and irradiated according to the parameters described in Table S9. After cooling to room temperature, the resulting solid was filtered and washed three times with cold ethanol. After drying, the ligand $\mathbf{L_1}$ was isolated to give in 83% yield. ^{1}H-NMR (DMSO), δ (ppm): 8.65 (1H, s, N=C-H); 8.64 (1H, s), 8.51 (1H, d), 8.40 (1H, s), 7.71 (2H, m, H-Ar), 7.51 (2H, m, H-Ar), 7.09 (1H, d), 6.63 (2H, d), 6.44 (2H, d), 6.28 (2H, dd), 3.31 (8H, q, NCH_2CH_3), 1.14 (12H, t, NCH_2CH_3). ^{13}C-NMR ($CDCl_3$), δ (ppm): 165.12, 158.82, 153.75, 153.20, 151.97, 149.03 (N=C-H), 144.88, 137.81, 133.77, 128.69, 128.42, 127.93, 124.21, 123.98, 123.54, 122.72, 120.71, 120.04, 108.00, 105.32, 98.01, 66.01 (spiro carbon), 44.35 (NCH_2CH_3), 12.61 (NCH_2CH_3).

Synthesis of compound L_2: A mixture of **1** (100 mg, 0.219 mmol), 3-formyl-6-methylchromone (41mg, 0.218 mmol), and ethanol (2 mL) was placed in a 10 mL reaction vial. The resulting mixture was stirred to make it homogeneous and it was placed in the cavity of a CEM microwave reactor. The closed reaction vessel was run under pressure and irradiated according to the parameters described in Table S10. After cooling to room temperature, the resulting solid was filtered and washed three times with cold ethanol. After drying, the ligand $\mathbf{L_2}$ was isolated to give in 87% yield. ^{1}H-NMR ($CDCl_3$), δ (ppm): 8.65

(1H, s, N=C-H); 8.40 (1H, s), 8.90 (1H, d), 8.81 (1H, s), 7.41 (2H, m, H-Ar), 7.30 (2H, m, H-Ar), 7.09 (1H, d), 6.44 (4H, H-Ar), 6.28 (2H, dd), 3.30 (8H, q, NCH_2CH_3), 2.32 (3H, s), 1.14 (12H, t, NCH_2CH_3). ^{13}C-NMR ($CDCl_3$), δ (ppm): 175.59, 165.01, 153.38, 153.81, 153.21, 152.94, 149.03, 149.88 (N=C-H), 140.46, 135.40, 134.83, 133.44, 128.93, 128.25, 127.88, 125.25, 123.81, 119.65, 117.95, 107.95, 105.71, 105.69, 98.10, 66.02 (spiro carbon), 44.32 (NCH_2CH_3), 20.93, 12.65 (NCH_2CH_3).

3. Results and discussion

3.1. Synthesis

The classical synthetic protocol to synthesize rhodamine compounds involves the reaction of rhodamine B with hydrazine hydrate (79%) in ethanol (phase I), followed by condensation of the resulting rhodamine B hydrazide **1** with chromone aldehydes also in ethanol (phase II), as is described in scheme 1. The reaction conditions for the microwave-assisted synthesis of rhodamine compounds (**L_1** and **L_2**) are summarized in Table S9 and Table S10, respectively. The work-up was easy and the products were obtained in excellent to moderate yields. Most significant are the substantially decreased reaction time, mild reaction conditions, no side reactions, and simplicity of the reaction procedure. Structural elucidation of synthesized compounds was carried out by means of FTIR and NMR spectroscopy.

3.2. Photophysical studies

The absorption spectra of **L_1** and **L_2** with Cu^{2+} were investigated by spectrophotometric titration in aqueous acetonitrile Tris-HCl buffer (10 mM, pH 7.2). The colorless solutions showed no absorption above 450 nm, properties which are characteristic of the predominant ring-closed spirolactam. This was further confirmed by the ^{13}C NMR signal at δ 66.01 and δ 66.02 for compound **L_1** and **L_2** respectively. However, upon addition of Cu^{2+} ion, a new absorption band at 560 nm appeared with a shoulder at 520 nm, and absorbance increased with increasing Cu^{2+} concentration, which can be ascribed to the formation of the ring-opened amide form of **L_1** and **L_2** upon Cu^{2+} ion binding (Fig.1). Meanwhile, the titration solutions turned pink instantaneously because of the ring-open structure caused by Cu^{2+} binding, suggesting that both compounds can serve as a naked-eye indicator for Cu^{2+} ions. No significant change in the UV-Vis spectrum was observed upon the addition of a 5-equivalent excess of other metal ions of interest: Na^+, K^+, Mg^{2+}, Ca^{2+}, Ni^{2+}, Zn^{2+}, Co^{2+}, Hg^{2+}, Pb^{2+}, Fe^{2+}, Fe^{3+}, Cr^{2+} and Cu^{2+}. The absorption profile of **L_2** was very similar to sensor **L_1**: again Cu^{2+} registered the highest absorption enhancement while little interference from Cr^{3+} and Ni^{2+} in the absorption spectra (Fig.S2). Therefore, both compounds exhibited high selectivity for Cu^{2+} over other metal ions.

The fluorescence responses of compound **L_1** and **L_2** to most metal ions were conducted by adding 5 equivalent of different metal ions respectively to the aqueous acetonitrile solutions. The fluorescence spectra were obtained by excitation at 510 nm, and both the excitation and emission slit were 5 nm. The sensors exhibited similar fluorescence spectroscopic properties upon binding with Cu^{2+}. The fluorescence emission wavelengths for **L_1** and **L_2** sensors appeared at 580 nm and 578 nm, respectively (Fig.2a and Fig.S3). This remarkable fluorescence enhancement was reasonably attributed to the existing conjugated xanthene

tautomer of the rhodamine moiety of compounds **L_1** and **L_2** [29]. There was a significant fluorescence emission intensity enhancement with 5 equivalents of Cu^{2+} which indicates that compound **L_1** is an excellent turn-on sensor for Cu^{2+}. Under the same conditions, we explored the sensitivity measurement of ion sensors. As shown in Fig.S4, rhodamine B derivative with nitro group exhibit excellent sensitivity towards copper ion. The fluorescence turn-on rates are observed to increase by a factor of six as the substituent is turned from methyl to nitro. Comparison of the fluorescence spectra of sensors **L_1**-Cu^{2+} and **L_2**-Cu^{2+} further confirmed the important role of substituents on the chromone ring. Therefore, we prefer to select electron-withdrawing substituent to detect metal ion that reveal high sensitivity. Thus, only **L_1** was chosen for further discussion, and the optical spectra of **L_2** are shown in the supporting information.

3.3. Fluorescence titration studies

The change in fluorescence emission spectrum was explored upon the addition of increasing concentrations of Cu^{2+}. Upon addition of Cu^{2+}, the fluorescence intensity increased in a Cu^{2+} concentration-dependent way as shown in Fig. 2b, accompanied with an obvious orange fluorescent enhancement. From the emission titration experiment, the association constant (k_a) of **L_1** with Cu^{2+} was estimated to be $3.12 \times 10^4\ M^{-1}$. Based on the fluorescence titration experiments, the limit of detection of **L_1** for sensing Cu^{2+} was calculated and it was found to be 2.11 μM.

3.4. Binding studies

To confirm the stoichiometry between sensor and Cu^{2+}, the method of continuous variation (Job's plot) was used [30]. During this experimental process, the total concentration of sensor and Cu^{2+} was kept constant at 50 μM, with a continuous variable molar fraction of guest $[Cu^{2+}]/([\text{sensor}] + [Cu^{2+}])$. As shown in Fig. 3, the plot of absorbance at 560 nm as a function of mole fraction of added Cu^{2+} ion reveals that both sensors bind to copper ion in 1:1 stoichiometry. The proposed binding mode of **L_1** is shown in Scheme 2.

3.5. pH studies

The fluorescence response of sensors was investigated under various pH conditions. As the pH decreases, the fluorescence intensity of **L_1** and **L_2** increases which could be ascribed to the spirolactum ring opening of the sensors due to the strong protonation [31]. Fig. S5 and S6 showed that for free sensors at $pH^{<}5$, due to protonation of the open-ring of spirolactam, an obvious color change and fluorescence turn-on appeared. Thus, all the optical measurements were performed in buffer solution with a pH of 7 to keep the sensors in their ring closed form. These results indicated that, the sensors can be applied for environmental and biological samples.

3.6. NMR and IR studies

^1H NMR spectra of **L_1** and **L_1** in the presence of one equivalent of Cu^{2+} have been recorded in DMSO-d_6. Various aromatic protons appear in the range of 6–9 ppm. The partial ^1H NMR spectrum of **L_1** shows the signal at 8.44 ppm corresponds to imine hydrogen which gets shifted up-filled with the addition of one equivalent of Cu^{2+} ions. Nevertheless, almost

no spectral changes were observed in other proton signals with addition of Cu^{2+} (Fig. 4). The characteristic peak of the amide carbonyl $\nu_{(C=O)}$ shifted from 1652 cm^{-1} to 1642 cm^{-1} in the presence of Cu^{2+}, indicating that carbonyl O atoms of the **L_1** involved in the coordination of Cu^{2+} (Fig. S10). Band at 1595 cm^{-1} is attributed to the presence of C=N moiety in free compound and that band is shifted to 1590 cm^{-1} in Cu^{2+} complex indicating retention of the C=N bond in the complex. These results suggested that the imine N, rhodamine carbonyl O, and chromone carbonyl O atoms participated in the coordination with Cu^{2+}.

3.7. Detection of cyanide (CN^-)

It was interesting to investigate the reversible binding nature of the sensor **L_1** as shown in Fig. 5a and scheme 2. It is very exciting and noteworthy that sensor **L_1** could be regenerated only by adding CN^- to the solution containing **L_1**-Cu^{2+}. Common anions, such as Cl^-, I^-, F^-, ClO_4^-, CH_3COO^-, HSO_4^-, $H_2SO_4^{2-}$, PO_4^{3-}, SCN^-, S^{-2}, HS^-, and OH^-, did not generate the same results. Due to the high stability of $Cu(CN)_2$, the **L_1**-Cu^{2+} complex could be serving as a possible means to detect CN^-. The addition of CN^- to the **L_1**-Cu^{2+} solution led to a change in color of the solution from pink to colorless, which was observed with the naked eye. The addition of CN^- to **L_1**-Cu^{2+} solution resulted in the reversal of the Cu^{2+} induced changes in the emission band at 580 nm in the fluorescence emission spectra. Thus, results strongly support that **L_1**-Cu^{2+} binds CN^- ions with higher selectivity and the process is reversible. Fig.5b shows that the intensity of the fluorescence emission decreases with increasing concentration of cyanide anion. The proposed binding mechanism of sensor **L_1** with Cu^{2+} in the presence and absence of CN^- was shown in Scheme 2.

3.8. Computational Studies

Time-dependent density functional theory (TD-DFT) calculations using the B3LYP functional and the 6–31G(d,p) basis set in the gas phase, and in a simulated water medium using a conductor like polarizable continuum (CPCM) model to obtain vertical UV-Vis electronic excitation data on sensors **L_1** and **L_2** and their respective Cu^{2+} complexes **L_1**-Cu^{2+} and **L_2**- Cu^{2+}. Also, emission data for the respective Cu^{2+} complexes in simulated acetonitrile were obtained. Atomic coordinates of the optimized structures were obtained from Spartan ‘18 software and then used as input to obtain both Spartan ‘18 (TDA) and Gaussian ‘09 (TD) data on said complexes. Spartan and Gaussian calculations of Cu^{2+} complexes showed excellent agreement. Wavelengths and oscillator strengths(f) for prominent vertical electronic excitations, as well as emission data for sensors and Cu^{2+} complexes are highlighted below.

In the gas phase for **L_1**, the most intense transition occurs at 408.19 nm with f=0.1274, and the energy gap between the highest occupied molecular orbital (HOMO = −5.11 eV) and the lowest unoccupied molecular orbital (LUMO= −2.48 eV) is 2.63 eV (λ = 471.42 nm). In water, this gap is 2.27 eV (λ = 546.19 nm), and HOMO is −5.04 eV and LUMO is −2.77 eV, and the most intense transition is 446.16 nm (f = 0.0050). For **L_1**-Cu^{2+} in the gas phase, the most intense transition is 734.37 nm (f = 0.0050) and the frontier orbital gap is 1.65 eV (751.42 nm, HOMO = −9.74 eV and LUMO = −8.09 eV). In water, this gap is 2.36 eV (525.36 nm, HOMO =5.55 eV, LUMO =3.19 eV) compared to 1.65 eV in the gas phase.

However, in water the dominant vertical excitation for **L_1**-Cu^{2+} occurs at 587.88 nm (f = 0.0035). For **L_1**, in both the gas phase and in water, HOMO is delocalized primarily over the entire xanthene moiety and the nitrogen of the two amino substituents while LUMO is delocalized over the oxo-chromene moiety and the nitro group with some electron density found on the nitrogen of the imine group. In the case of **L_1**- Cu^{2+}, similar electron density distribution is found for HOMO and LUMO in both gas and water (Fig. 6 and 7)

In the gas phase for **L_2**, the most intense transition occurs at 320.21nm (f=0.5252), and in water at 322.19 nm (f=0.6298). Also, in the gas phase, the frontier energy gap for **L_2** is 3.62 eV (λ = 342.50 nm, HOMO = −5.03 eV and LUMO= −1.41 eV), and in water, this gap is 3.25 eV (381.49 nm, HOMO = −5.07 eV and LUMO = −1.82 eV). In the gas phase for **L_2**-Cu^{2+}, the most intense transition occurs at 659.37 nm (f=0.0070); the HOMO-LUMO energy gap is 2.11 eV (587.60 nm, HOMO = −9.67 eV and LUMO = −7.56 eV). In water, the dominant vertical excitation is 593.60 nm (f=0.0040). The HOMO-LUMO energy gap is 2.81 eV (441.22 nm) with HOMO = −5.55 eV and LUMO is −2.74 eV. For **L_2** in both gas and water, HOMO is found primarily on half of the xanthene moiety, and LUMO is found throughout the oxo-chromene moiety, imine group, the spirolactam ring and the connecting benzene ring. For **L_2**-Cu^{2+} in gas, HOMO is delocalized over the entire xanthene moiety and the two amino substituents. LUMO is delocalized over the oxo-chromene moiety. For **L_2**-Cu^{2+} in water, both the HOMO and the LUMO are found over the xanthene moiety, however, in the HOMO there is a separation at the xanthene oxygen and the carbon para to it, but no separation exists in the LUMO (Fig. S14–15).

In simulated acetonitrile for **L_1**- Cu^{2+}, the most intense absorption transition occurs at 442.11 nm (f=1.3137); the HOMO-LUMO energy gap is 2.35 eV (527.59 nm, HOMO = −5.61 eV and LUMO = −3.26 eV) (Fig. S16). As in the case in both the gas phase and water, HOMO is delocalized primarily over the entire xanthene moiety and over the nitrogens of the two amino substituents while LUMO resembles more of the LUMO of **L_1**-Cu^{2+} in water. Also, in simulated acetonitrile, the most intense emission peak in the fluorescent spectrum of **L_1**-Cu^{2+} is at 707.76 nm (f=0.0074). In the same medium, for **L_2**-Cu^{2+}, the most intense absorption transition occurs at 441.03 nm (f=1.3953); the HOMO-LUMO energy gap is 2.82 eV (439.66 nm, HOMO = −5.60 eV and LUMO = −2.78 eV) (Fig. S17); and both frontier orbitals HOMO and LUMO of **L_2**-Cu^{2+} in acetonitrile resemble their counterparts in water, respectively. The most intense emission peak for **L_2**-Cu^{2+} is at 695.87 (f=0.0078).

4. Conclusion

In conclusion, two rhodamine derivatives with different substituents groups have been synthesized for the detection of copper ions in aqueous acetonitrile solution. Sensor **L_1** showed fast response, good selectivity and sensitivity toward Cu^{2+} in aqueous solution. Sensor **L_1** could be used as a potential material for Cu^{2+} recognition in a low concentration. These studies show that compared with the methyl unit (-CH_3), the introduction of nitro (-NO_2) groups to chromone unit of compound **L_1** can significantly improve sensitivity and selectivity to copper ion. The in situ prepared **L_1**-Cu^{2+} complex was used to detect CN^- via the metal-displacement approach which displayed an excellent selectivity and sensitivity towards CN^-.

Supplementary Material

Refer to Web version on PubMed Central for supplementary material.

Acknowledgements

This work was supported by the National Institute of General Medical Sciences of the National Institutes of Health under Award Number SC2GM125512 and Morgan State University.

Reference

[1]. Malvankar L, Shinde M, Ion-pair extraction and determination of copper (II) and Zinc (II) in environmental and pharmaceutical samples, Analyst, 116 (1991)1081–1084. [PubMed: 1801605]

[2]. Bull C, Thomas R, Rommens J, Forbes R, Cox W, The Wilson disease gene is a putative copper transporting p-type ATPase similar to the menkes gene, Nat. Genet 5 (1993) 327–337. [PubMed: 8298639]

[3]. Vogt K, Mellor J, Tong G, Nicoll R, The action of synaptically released Zinc at hippocampal mossy fiber synapses, Neuron, 26 (2000) 187–196. [PubMed: 10798403]

[4]. Barnham K, Masters C, Bush A, Neurodegenerative disease and oxidative stress. Nat. Rev. Drug Discov 3 (2004) 205214.

[5]. Waggoner D, Bartnikas T, Gitlin J, The role of copper in neurodegenerative disease. Neurobio. 6 (1999) 221.

[6]. Brown D, Kozlowski H, Biological inorganic and bioinorganic chemistry of neurodegeneration based on prion and Alzheimer diseases. Dalton Trans. 13, (2004) 1907.

[7]. Liu Z, Zhang C, Wang X, He W, Guo Z, Design and synthesis of a ratiometric fluorescent chemosensor for Cu (II) with a fluorophore hybridization approach, 14 (2012) 4378.

[8]. Liu Z, Yang Z, Li T, Wang B, Li Y, Quin D, Wang M, Yan M., An effective Cu(II) quenching fluorescence sensors in aqueous solutions and 1D chain coordination polymer framework, Dalton Transaction, 40 (2011) 9370.

[9]. Sung H, Kwm P, Lee J, Kim J, Hong C, Kim J, yan S, Lee J, Joo T, Coumarin-derived Cu^{2+}-selective fluorescence sensor: Synthesis, mechanism, and applications in living cells, J. Am. Chem. Soc, 132 (2009) 2008.

[10]. Liu J, Yang J, Chan C, Huang Z, A new fluorescent chemosensor for Fe^{3+} and Cu^{2+} based on Calix [4] arene, Tetrahedron Lett, 43 (2002) 9209.

[11]. Weerasinghe A, Abebe F, Sinn E, Rhodamine based turn-on dual sensor for Fe^{3+} and Cu^{2+}, Tetrahedron letters, 52 (2011) 5648.

[12]. Hue FJ, Su J, Sun YQ, Yin CX, Tong HB, Nie ZX, A rhodamine-based dual chemosensor for the visual detection of copper and the ratiometric fluorescent detection of vanadium, Dyes and Pigments, 86 (2010) 50.

[13]. Abebe F, Sinn E, Fluorescein-based fluorescent and colorimetric chemosensors for copper in aqueous media, Tetrahedron letters, 52 (2011) 5234.

[14]. Xuan Z, Yasuhiro S, Takayuki H, Cu(II)-selective green fluorescence of a rhodamine- diacetic acid conjugate, Org. Lett 9 (2007) 5039–5042. [PubMed: 17975919]

[15]. Xiaoqiang C, Min J, Hanyoung L, Songzi K, Jeesun L, Seong-Won N, Sungsu P, Kwan-Mook K, Juyoung Y, New fluorescent and colorimetric chemosensors bearing rhodamine and binaphthyl groups for the detection of Cu^{2+}, Sensors and Actuators B 137 (2009) 597–602.

[16]. Ming D, Tian-Hua M, Ai-Jiang Z, Yu-Man D, Ya-Wen W, Yu P, A series of highly sensitive and selective fluorescent and colorimetric ‘off-on” chemosensors for Cu(II) based on rhodamine derivatives, Dyes and Pigments, 87 (2010) 164–172.

[17]. Xinqi C, Huimin M, A selective fluorescence-on reaction of spiro form fluorescein hydrazide with Cu(II), Analytical Chimica Acta 575 (2006) 217–222.

[18]. Manoj K, Naresh K, Vandana B, Parduman S, Tandeep K, Highly selective fluorescence Turn-on chemodosimeter based on rhodamine for nanomolar detection of copper ions, 14 (2012) 406.

[19]. Zhang Z, Zhang Y, Hang W, Yan X, Zhao Y, Sensitive and selective off-on rhodamine hydrazide fluorescent chemosensor for hypochlorous acid detection and bioimaging, 85 (2011) 779.

[20]. Weerasinghe AJ, Abebe FA, Venter A, Sinn E, Rhodamine based turn-on sensors for Cr^{3+} and Ni^{2+}: detecting CN^{-} via the metal displacement approach of sensor-Cr^{3+} complex, Journal of Fluoresc, 26 (2016) 891.

[21]. Huang J, Xu Y, Qian X, A rhodamine-based Hg^{2+} sensor with high selectivity and sensitivity in aqueous solution: A NS2-containing receptor, J. Org. Chem 74 (2009) 2167. [PubMed: 19209877]

[22]. Li L, Fang Z, A novel “turn on” glucose-based rhodamine B fluorescent chemosensor for mercury ions recognition in aqueous solution, Spectroscopy letters, 58 (2014) 578.

[23]. Leite A, Silva AM, Cunha-Silva L, De Castro B, Gameiro P, Rangel M, Discrimination of fluorescence light-up effects induced by P^{H} and metal ion chelation on a spirocyclic derivative of rhodamine B, Dalton Trans., 42 (2013) 6110. [PubMed: 23299402]

[24]. Weerasinghe AJ, Schmiesing C, Sinn E, Highly sensitive and selective reversible sensor for the detection of Cr^{3+}, Tetrahedron Lett. 50 (2009) 6407–6410

[25]. Weerasinghe AJ, Schmiesing C, Sinn E, Synthesis, characterization, and evaluation of rhodamine based sensors for nerve gas mimics, Tetrahedron 67 (2011) 2833–2838.

[26]. Du W, Cheng Y, Shu W, Wu B, Kong Z, Qi Z, The influence of different substituents on spectral properties of rhodamine B based chemosensors for mercury ion and application in EC 109 cells, Can. J. Chem 95 (2017) 751–757.

[27]. Abebe F, Sinn E, E. Fluorescein-based fluorescent and colorimetric chemosensors for copper in aqueous media, Tetrahedron Lett. 52 (2011) 5234–5240.

[28]. Xiang Y, Tong A, Jin Peiyuan, Ju Y, New fluorescent rhodamine hydrazine chemosensor for Cu(II) with high selectivity and sensitivity, Org. Lett 8 (2006) 2863–2863. [PubMed: 16774276]

[29]. Huang X, Lu Z, Wang Z, Fan C, Fan W, Shi X, Zhang H, Pei M, A colorimetric and turn-on fluorescent chemosensor for selectivity sensing Hg^{2+} and its resultant complex for fast detection of I- and S^{-2}, Dyes Pigm. 128 (2016) 33–40.

[30]. Li C, Qin, Wang B, Fan L, Yan J, Yang Z, A chromone-derived Schiff-base ligand as Al^{3+} turn on fluorescent sensor: synthesis and spectroscopic properties, J. Fluoresc 26 (2016) 345–353 [PubMed: 26545355]

[31]. Cui P, Jiang X, Sun J, Zhang Q, Gao F, A water-soluble rhodamine B-derived fluorescent for PH monitoring and imaging in acidic regions, Methods Appl. Fluoresc 5 (2017) 024009. [PubMed: 28452333]

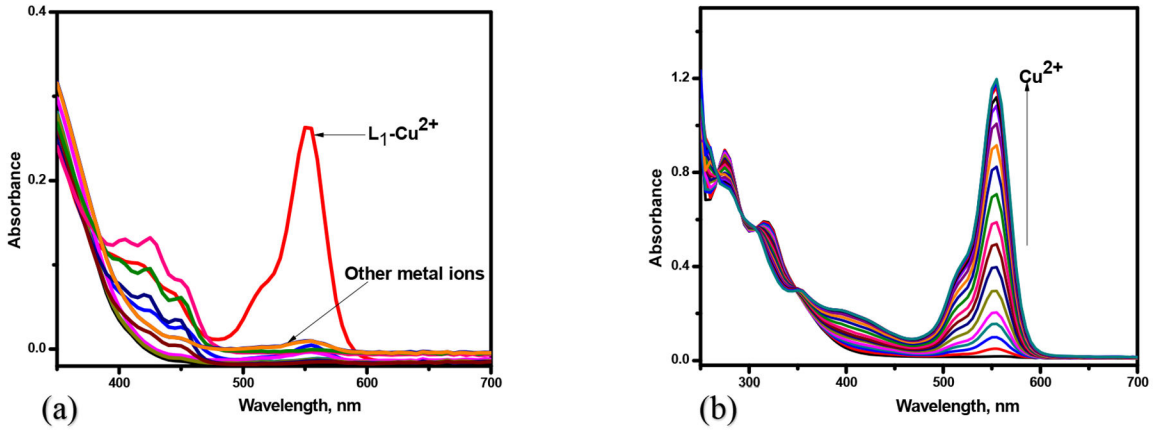

Fig. 1.

(a) UV-Vis spectra of **L_1** (10μM) with metal ions in CH_3CN/H_2O (7:3 v/v) solution. (b) UV-Vis spectra of **L_1** (10μM) with Cu^{2+} (0–20μM) in CH_3CN/H_2O (7:3 v/v) solution

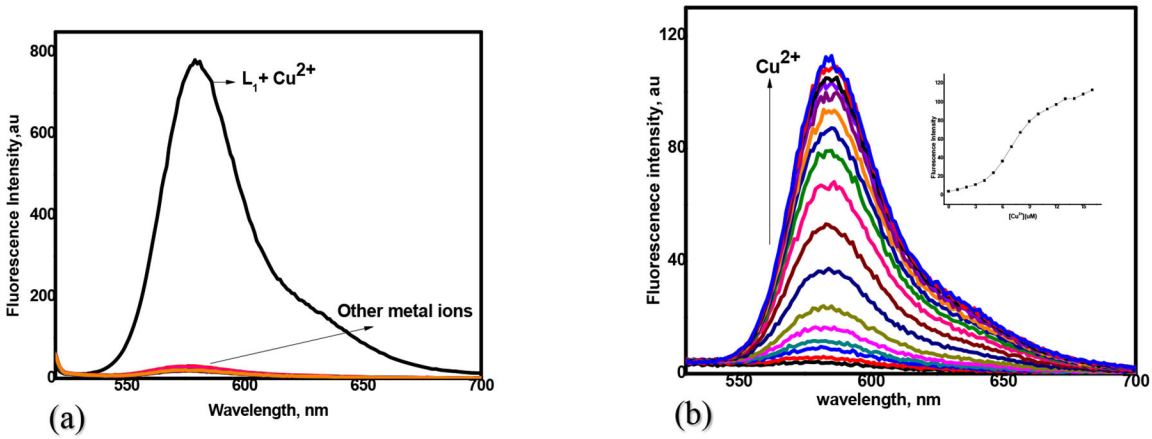

Fig. 2.

(a) Fluorescence spectra of **L_1** (20μM) with metal ions (20μM) in CH_3CN/H_2O (7:3 v/v) solution (λex=510 nm). (b) Fluorescence spectral titration of **L_1** (10μM) on the incremental addition of Cu^{2+} (0–5equiv) (λex=510 nm)

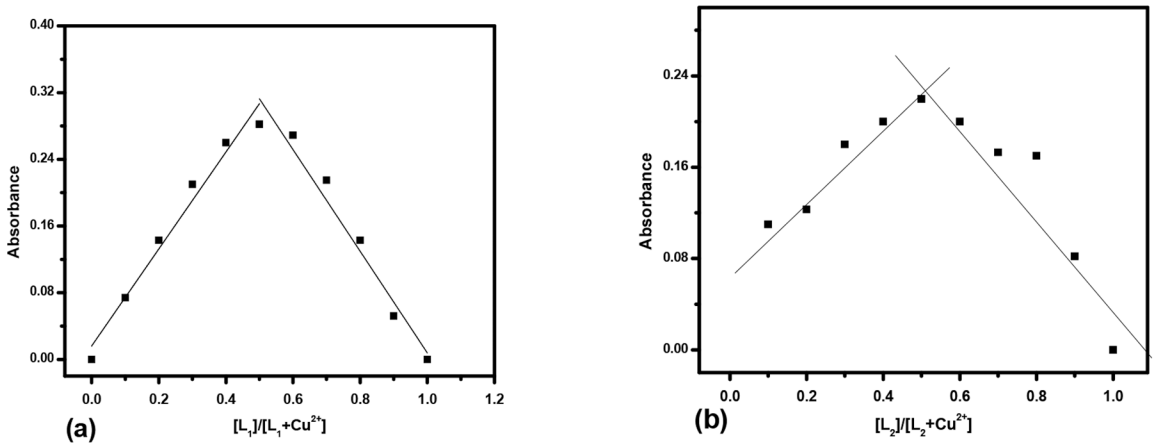

Fig. 3.

(a) Job's plot for determination of $\mathbf{L_1}$-Cu^{2+} complex (50 μM) in CH_3CN/H_2O (7:3 v/v) solution. (b) Job's plot for determination of $\mathbf{L_2}$-Cu^{2+} complex (50 μM) in CH_3CN/H_2O (7:3 v/v) solution.

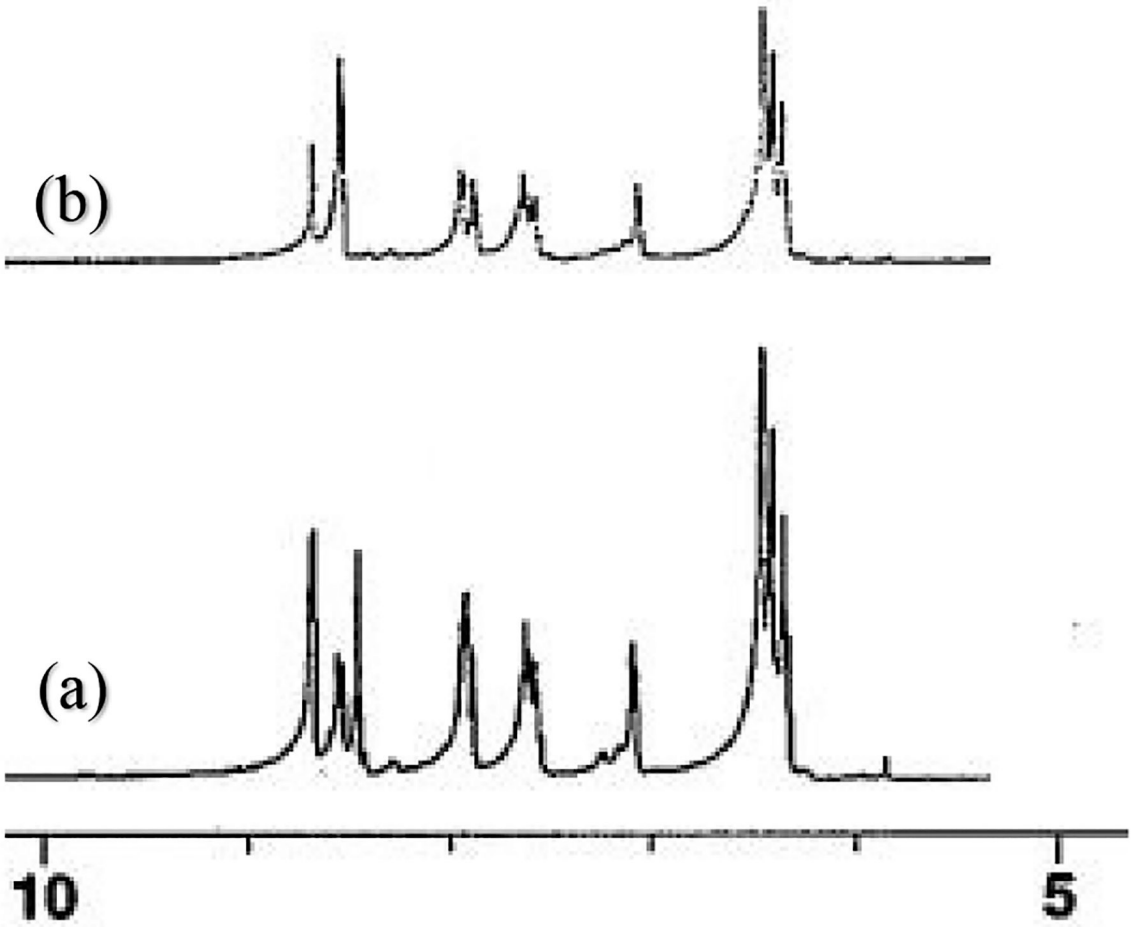

Fig. 4.
Partial ^{1}H NMR titration with Cu^{2+} ions in DMSO-d_6. [(**a**) $\mathbf{L_1}$ and (**b**) $\mathbf{L_1}$: Cu^{2+} (1:1)]

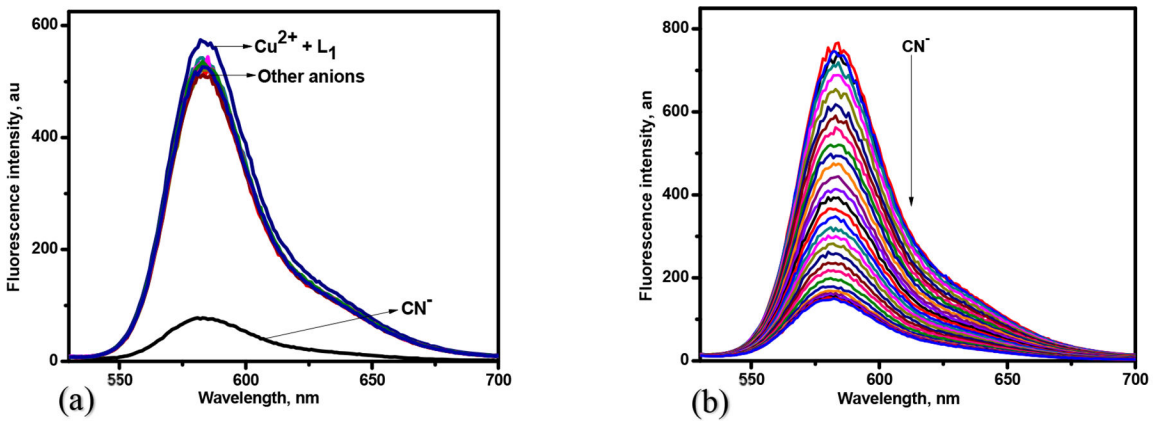

Fig. 5.

(a) Changes in the fluorescence spectra of $\mathbf{L_1}$-Cu^{2+} complex in presence of different anions. (b) Fluorescence spectra of $\mathbf{L_1}$ (20 μM) with copper ion upon addition of CN^- (0–5equiv) in in CH_3CN/H_2O (7:3 v/v) solution.

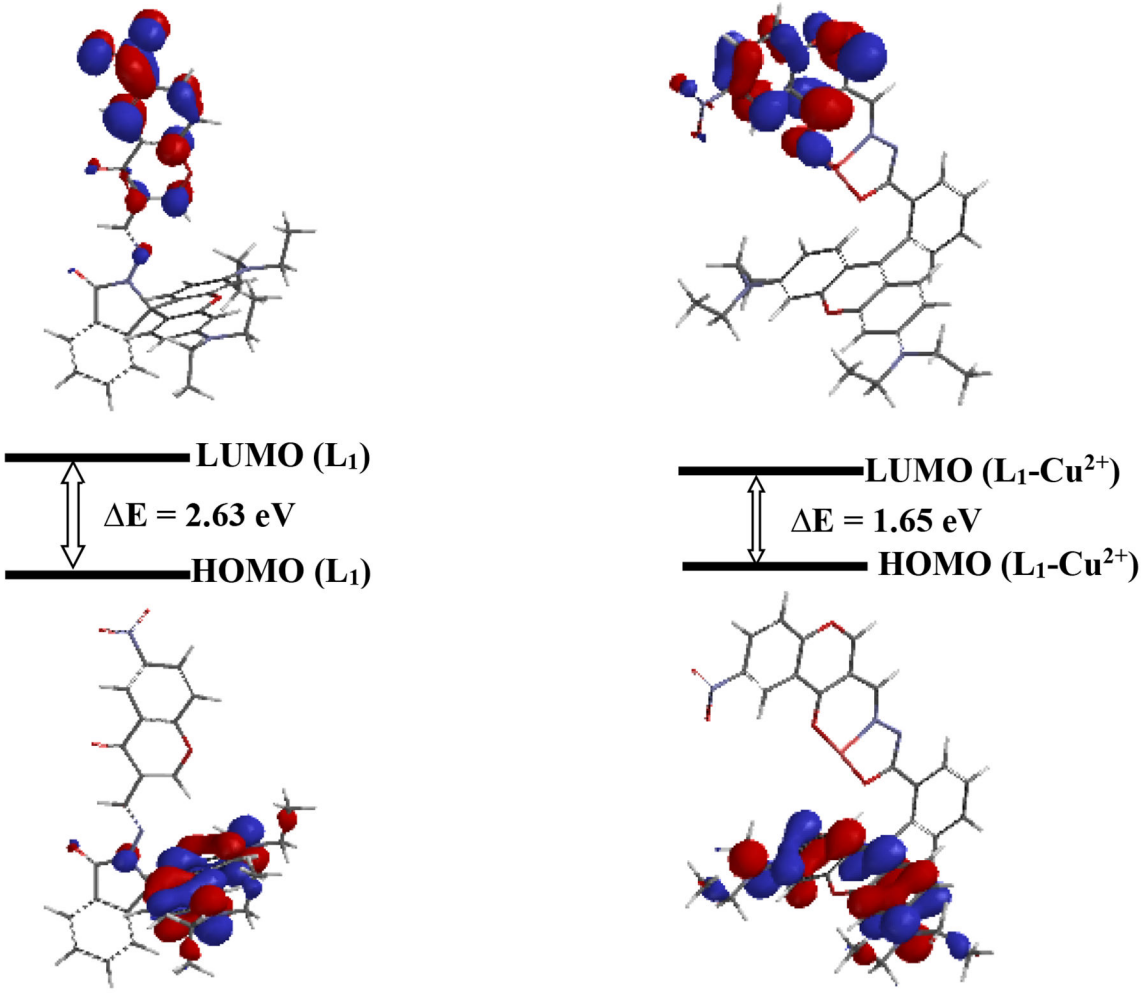

Fig. 6.

Electronic distribution of HOMO and LUMO energy levels for $\mathbf{L_1}$ and the $\mathbf{L_1}$-Cu^{2+} in gas phase

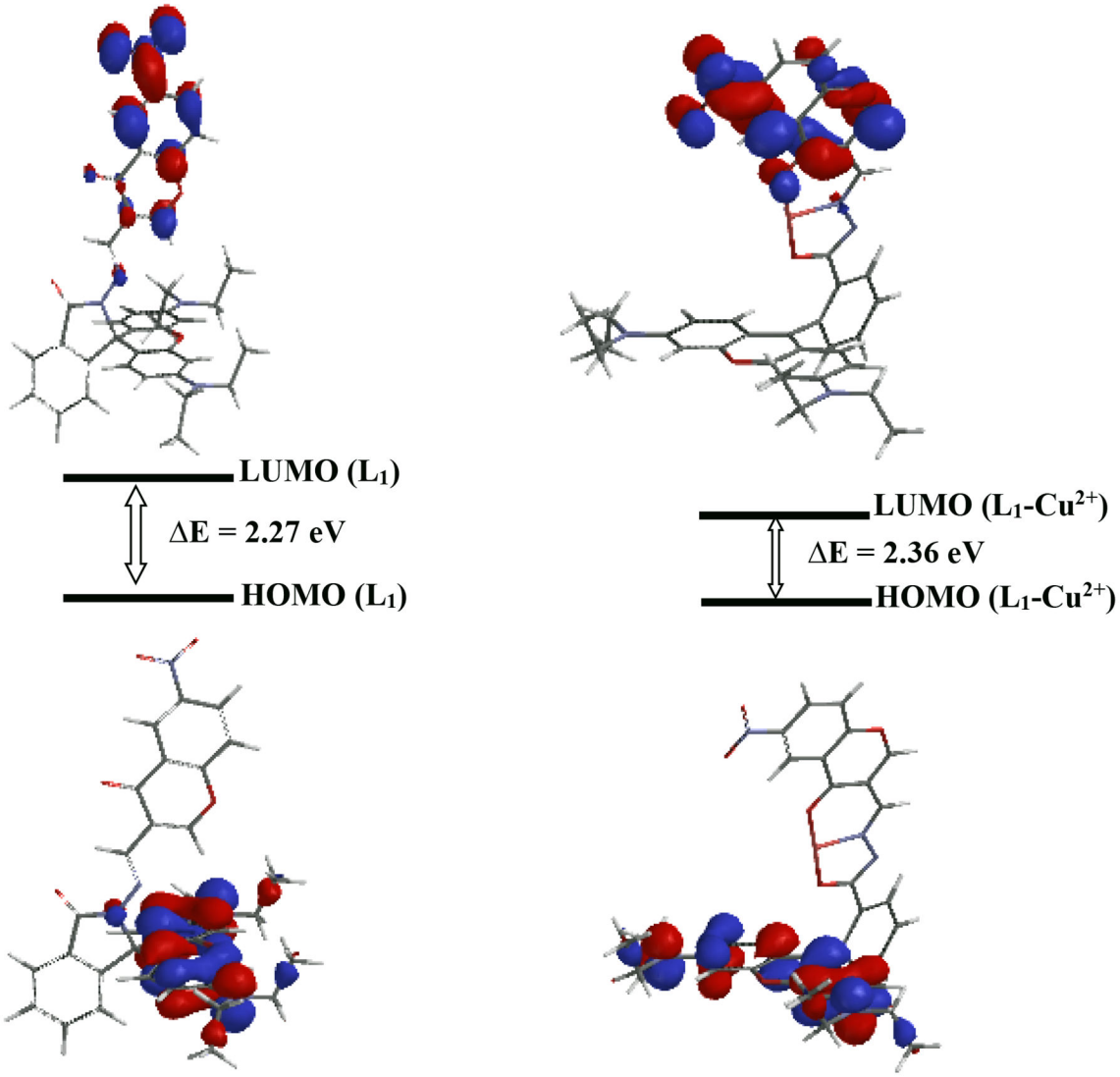

Fig. 7.
Electronic distribution of HOMO and LUMO energy levels for **L** and the $\mathbf{L_1}$-Cu^{2+} in water

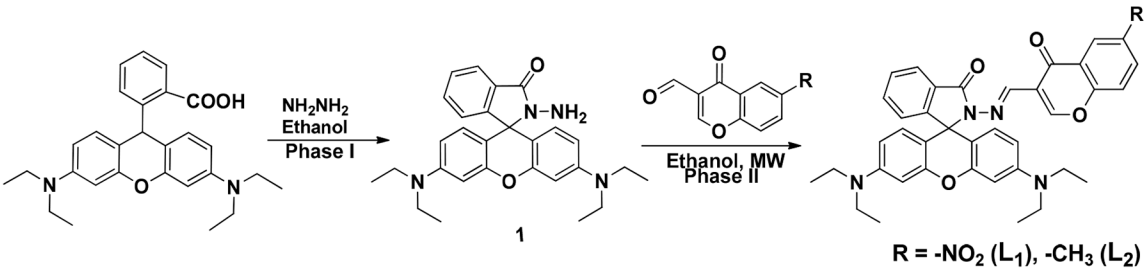

Scheme 1.
Chemical structure and synthetic route of $\mathbf{L_1}$ and $\mathbf{L_2}$

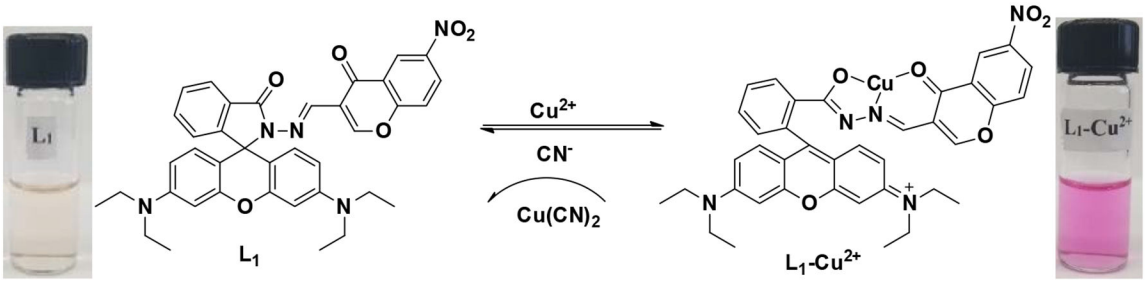

Scheme 2.

A possible proposed binding mechanism of sensor $\mathbf{L_1}$ towards Cu^{2+} in the presence and absence of cyanide ion.